Journal of Applied Sciences and Nanotechnology

Journal homepage: jasn.uotechnology.edu.iq

Synthesis and Evaluation of Bi_2WO_6-MWCNT Nanocomposites for Antibacterial Applications against Multidrug-Resistant Pseudomonas Aeruginosa

[1,2]Zeena R. Rhoomi, [1]Duha S. Ahmed*, [1]Majid S. Jabir, [3]Anjan Kumar

[1]Department of Applied Sciences, University of Technology – Iraq
[2]Ibn Sina University of Medical and Pharmaceutical Science – Iraq
[3]Department of Electronics and Communication Engineering, GLA University – India

A R T I C L E I N F O

Article history:
Received: January, 25, 2024
Accepted: April, 24, 2024
Available online: June, 10, 2024

Keywords:
MWCNTs,
Bi_2WO_6,
Hydrothermal method,
Antibacterial activity,
Antibiofilm

Corresponding Author:
D. S. Ahmed
duha.s.ahmed@uotechnology.edu.iq

A B S T R A C T

Bismuth tungstate (Bi_2WO_6) is an aurivillius oxide with potential as a visible light-active photocatalyst. However, its wide band gap limits absorption of visible light. Decoration with multi-walled carbon nanotubes (MWCNTs) has been shown to enhance photocatalytic properties. This study reports the hydrothermal synthesis of pure Bi_2WO_6 and Bi_2WO_6-MWCNT nanocomposites using a 1:2.5 molar ratio of Bi_2WO_6:MWCNTs. Fourier transform infrared spectroscopy, field emission scanning electron microscopy, and energy dispersive X-ray spectroscopy analysis were used to characterize the morphology, chemical bonding, and composition. Adding MWCNTs reduced particle size, increased surface area, and prevented aggregation. Antibacterial testing showed the Bi_2WO_6-MWCNT nanocomposite inhibited Pseudomonas aeruginosa, a multidrug-resistant bacterium, more effectively than pure Bi_2WO_6. Investigation of morphology and bonding revealed the influence of decorated and embedded MWCNTs on bismuth components and particle size. Enhanced antibacterial and anti-biofilm activity of the nanocomposite may be due to increased oxidative stress from reactive oxygen species generation. This facile hydrothermal method synthesizes a Bi_2WO_6-MWCNT nanocomposite combining the properties of both materials, showing promise for biomedical applications.

https://doi.org/10.53293/jasn.2024.7258.1272, Department of Applied Sciences, University of Technology - Iraq.

1. Introduction

In recent years, Bismuth tungsten (Bi_2WO_6) nanoparticles have garnered significant interest because of the potential photocatalytic activity in visible regions [1-5]. The Bi_2WO_6 is one of aurivuillius type oxide and represents a distinctive semiconductor photocatalyst with a small band gap (2.8eV), therefore could work under visible light (sunlight) compared to TiO_2 photocatalyst [6-8]. On the other hand, the studies have revealed the limited catalytic performance of Bi_2WO_6 because of the high molecular weight of Bi_2WO_6 compared to other compounds due to multiple elements in the chemical formula that prone to increase the recombination rate and reduced forming of active adsorption sites [9–14]. To overcome these limited, active strategies like doping, coupling with carbon compounds, and forming nanocomposites can be achieved [15-17]. Of these strategies, the hydrothermal method is the most widely synthesis technique, and it's achieved in a sealed container to facilitate the reaction between the precursors in water-based solution at high pressure and temperature, achieving controlling particle size and shape with less expensive [18-22]. Recently, carbon nanotubes (CNTs) are more effective and applicable compared to other nanoparticles due to their outstanding high aspect ratio, electron transfer capability, large surface area, and high surface chemical functionality [23-24]. Specifically, the multi-walled carbon nanotubes (MWCNTs) are regarded as a viable material for the environmental field and are attractive options for the delivery of biomolecules and drugs in biomedical applications [25-27]. The reason of MWCNTs have received a lot of attention represented by high aspect ratio, which result in increasing their adsorption and conjugated to other semiconductor materials (like Bi_2WO_6) and forming nanocomposite with high adsorption sites compared to pure Bi_2WO_6. Furthermore, MWCNTs are characterized by needle shapes and tunable functionalization, which improve antibacterial activity as a result of their significant interaction with bacterial cells. Since bacterial death is related to the oxidative stress mechanism generated by reactive oxygen species (ROS) [28-33].

Our work represented a facile synthesis of Bi_2WO_6 and Bi_2WO_6/MWCNTs nanocomposite at a molar ratio of 1:2.5 Bi_2WO_6: MWCNTs using a hydrothermal method. The morphology and chemical bonding of pure Bi_2WO_6 and nanocomposite were investigated, showing the influence of decorated and embedded MWCNTs with bismuth components and revealing the average particle size of nanocomposite compared with pure Bi_2WO_6. Moreover, Bi_2WO_6/MWCNTs nanocomposite exhibited high antibacterial and ant-biofilm properties against multidrug-resistance bacterium like gram-negative P. aeruginosa compared to Bi_2WO_6, making them promising for biomedical applications.

2. Materials and Method

2.1. Materials

Bismuth nitrate pentahydrate with purity 98% (Bi $(NO_3)_3$ $5H_2O$) was supplied from the Sigma-Aldrich. Besides, Sadium tungstate dehydrate $Na_2WO_4.2H_2O$ was purchased from Sigma-Aldrich, Hexadecyltrimethylammonium CTAB, nitric acid (HNO_3) where purchased from CDH Company, India. Sodium hydroxide (NaOH) was supplied from chemical reagent. The deionized water (DI) was used as the solvent throughout all of the procedures carried out in the study.

2.2. Synthesis of Bi_2WO_6 Nanostructure and Bi_2WO_6/MWCNTs Nanocomposite

Utilizing the hydrothermal method, pure Bi2WO6 nanostructure was prepared using 100 ml of Deionized water and mixed with 4mmol of Bi $(NO_3)_3.5H_2O$, 2 mmol of $Na_2WO_4.2H_2O$, and 0.1g of CTAB as catalyst agent. At room temperature, the mixture was mixed. For 1h using a magnetic stirrer and adjusted to a pH of 7. The resulting white suspension solution was sealed in a 100 ml Autoclave with a Teflon liner. After that, the autoclave was kept in an oven set at 180°C for 20 hours. The autoclave was allowed to cool to room temperature, resulting in the formation of a white precipitate. The resulting Bi_2WO_6 powder was subjected to a 10 hr oven drying process after being rinsed with ethanol and distilled water. The chemical **Eq. (1)** below of the resulted represent by:

$$2Bi(NO_3)_3.\ 5H_2O + 3Na_2WO_4.\ 2H_2O \longrightarrow Bi_2WO_6 + 6NaNO_3 + 17H_2O \qquad (1)$$

For Bi_2WO_6/MWCNTs nanocomposite, the molar ratio of Bi_2WO_6: MWCNTs was set as 1:2.5. Initially, 1 gram of functionalized F-MWCNTs and 0.4 gram of Bi_2WO_6 were mixed in 50 ml of deionized water. This mixture was stirred for 1hr in a beaker using a magnetic stirrer. To achieve dispersion, the mixture was dissolved using ultrasonication for 2 hrs. Simultaneously, 2 ml of 4M sodium hydroxide (NaOH) was dissolved in Deionized water by magnetic stirring at 25°C for 20 min. The Bi_2WO_6/MWCNTs solution was continuously stirred while the (NaOH) solution was added dropwise at 3 drops per minute until the pH reached 7. The final combination was subjected to a temperature of 180°C for 20 hours in a stainless-steel autoclave lined with Teflon, which could contain 150 ml. After that, it was time to let the autoclave drop to ambient temperature. The recovered residues underwent several washes with ethanol and water before being dried in a convection oven set at 60°C for 12 hours.

2.3. Identifying Characteristic

Field emission scanning electron microscopy (FESEM, TESCAN, MIRA3, Czeck) was used to analyze the morphology and structure of both pure Bi_2WO_6 and a Bi_2WO_6/MWCNTs nanocomposite with Energy Dispersive X-ray spectroscopy (EDS) used to define the composition elements of the resulted samples. By utilizing the FTIR spectrophotometer (8400S, Shimadzu) to determine the changes in the spectra after the addition MWCNTs in range between 500 and 4000 nm, we could learn more about the materials' bonding formation.

2.4. The Antibacterial Activity Assay

The antibacterial activity of Pure Bi2WO6 and Bi2WO6/MWCNTs nanocomposite (using molar ratio 1:2.5 of Bi_2WO_6: MWCNTs) was assessed by agar well diffusion assay against pseudomonas aeruginosa as gram's negative bacterial strains. Initially, about 20 mL of Muller-Hinton (MH) agar was aseptically poured into sterile Petri dishes. A sterile wire loop was used to capture the bacterial species isolated from wound infection. Wells on the agar plates with a diameter of 6 mm were drilled using the tips of sterile micropipettes after the organisms had been cultured. Overnight, bacterial samples with varying doses (62.5, 125, 250 µg/ml) were cultured on Muller-Hinton (MH) agar (HiMedia India) that included pure Bi2WO6 and a Bi_2WO_6/MWCNTs nanocomposite using a molar ratio of 1:2.5. A control strain of bacteria that was not treated was also included. The agar plates were photographed, and the inhibition zones were measured. The Data are represented as mean ±SD of three independent experiments.

2.5. Investigation Anitbiofilm Activity of Pure Bi_2WO_6 and Nanocomposite Bi_2WO_6: MMWCNTs 1:2.5

A control sample was prepared using untreated Lysogenia broth medium (HiMedia, India) culture plates, whereas samples treated with Bi_2WO_6 and nanocomposite at a concentration of 125 µg/mL for 24 hours were shown. The samples were subsequently stained using the FilmtracerTM live/deadTM biofilm viability Kit. A Leica TCS SP5 II confocal microscope was used to capture the image, which was then examined using flow cytometry. The proportion of untreated control cells was used to represent the outcomes of the biofilm bacteria's viability.

3. Results and Discussion

The chemical bonding of Bi_2WO_6 nanostructure and Bi_2WO_6/MWCNTs nanocomposites was determined using FTIR analysis in the 500-4000 cm^{-1} range. According to **Fig. 1**, pure Bi_2WO_6 nanostructure (blue line) prepared under the same condition reveals the stretching vibrations of the W-O, Bi-O stretching was linked to the strong bands seen at a frequency range of 500-1300 cm^{-1} [34-36]. The broader absorption band at 3455 cm^{-1} was identified as the result of stretching vibrations of -OH groups of adsorbed H_2O on the surface of the Bi_2WO_6 sample.

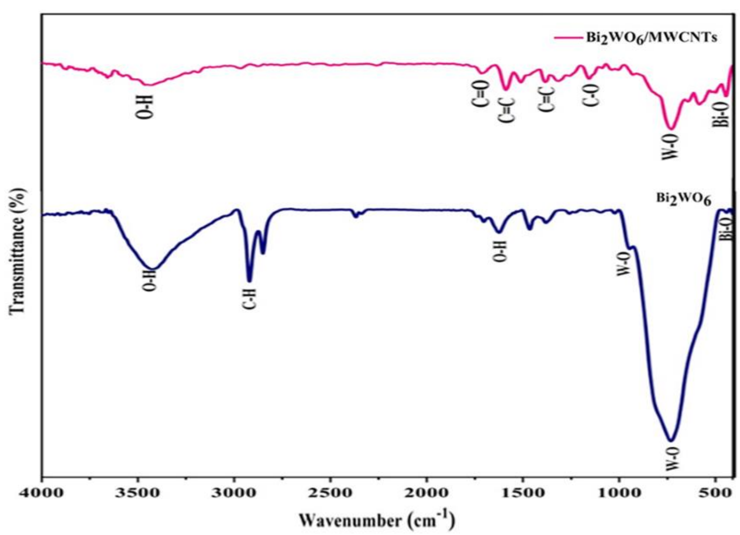

Figure 1: FTIR transmittance spectra of pure Bi_2WO_6 and Bi_2WO_6/MWCNTs 1:2.4 by hydrothermal method.

The vibration peak at 1624 cm^{-1} could be identified as the bending vibration of the O-H bond in the samples that were absorbing water molecules [37]. According to [38], the hydrothermal synthesis of CTAB occurs at 2921 cm^{-1} and 2854 cm^{-1}, which are related to the C-H stretching vibrations of the methyl and methylene groups, respectively.

The results shown in **Fig. 1** and **Table 1** indicate that these vibrations are consistent with the previous literature [39- 40]. Moreover, in the state of Bi_2WO_6/MWCNTs nanocomposite at a molar ratio of set as 1:2.5, The FTIR spectra from 500 to 4000 cm^{-1} are shown in **Fig. 1** (pink line). The peaks observed at 439-578 and 729 cm^{-1} corresponded to the stretching vibrations of Bi-O and W-O bonds, respectively [41]. The broad absorption band at 3441cm^{-1} was attributed to the stretching vibrations of O-H bonds on the sample's surface. The relatively weaker peaks within the 1153-1712 cm^{-1} range indicated functional groups associated with MWCNTs. Specifically, the peaks at 1153cm^{-1} was attributed to C-O stretching, while the peaks at 1377 and 1585.48 cm^{-1} were associated with the C=C stretching mode related to defects on the sidewalls of MWCNTs. Notably, the peak at 1712 cm^{-1} represented the C=O stretching mode in the Bi_2WO_6/MWCNTs nanocomposite [42].

Table 1: Transmission peak locations and wavenumber assignments were measured by FTIR measurements in the Bi_2WO_6 nanostructure and nanocomposite with a 1:2.5 molar ratio of Bi_2WO_6: MWCNTs.

Observed Modes (cm^{-1})		
Bi_2WO_6	**Bi_2WO_6/MWCNTs**	**Attribution**
731	729	WO_6 symmetric stretching
436	439-578	Bi-O Bending bonds
3455	3441	O-H stretching vibrations
162٤	1712	C=O stretching
-	1377-1508	C=C stretching vibration
-	1153	C-O stretching vibration

The morphology and microstructure of produced pure Bi_2WO_6 and Bi_2WO_6/MWCNTs nanocomposite with molar ratio 1:2.5 Bi_2WO_6: MWCNTs were examined using FESEM as shown in **Fig. 2 a,b**. The enlarged view in inset image scale 500 nm **Fig. 2 a**, shows that each particle has a flower-like structure composed of a group of 2D flakes that radiate in all directions.

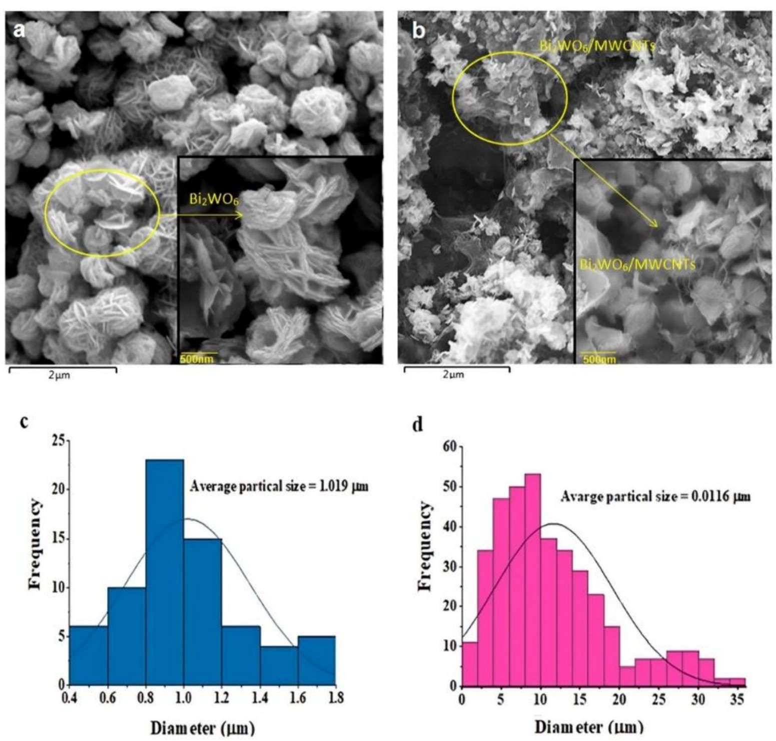

Figure 2: FESEM images of **a)** pure Bi_2WO_6 and **b)** Bi_2WO_6/MWCNTs nanocomposite at molar ratio 1:2.5 and average particle size using Image J, **c)** pure Bi_2WO_6 and **d)** Bi_2WO_6 /MWCNTs nanocomposite using hydrothermal method.

Besides, the orthorhombic pure Bi_2WO_6 was composed of flower-shaped particles with a diameter of about 1-2µm [43-44]. The resulting nanostructures are related to the Gibbs-Thomson law [45]. Moreover, nucleation processes are driven by the reduction of the system's total energy result in a relatively high surface area with bigger sizes under hydrothermal conditions to give Bi_2WO_6 nanoflakes structures [46]. **Fig. 2b** presents the Bi_2WO_6/MWCNTs nanocomposite morphology characteristics. The image reveals the presence of uniform spherical aggregates composed of cluster structures resembling layered nanoparticles. The inset image scale 500nm in **Fig. 2b**, reveals MWCNTs decorated Bi_2WO_6 surface and confirms the interaction between MWCNTs and the Bi_2WO_6 nanostructure. Furthermore, increasing the MWCNTs content to Bi_2WO_6 at a ratio of 1:2.5 resulted in embedded inside and on the surface of Bi_2WO_6 as shown in FESEM images [47-49]. Furthermore, the average particle size distribution of the Bi_2WO_6 particles was around 1.019 µm, and the average particle size of Bi_2WO_6/MWCNTs nanocomposite was about 0.0116 µm as determined by image J in **Fig. 2 c,d**. It is worth noting that FESEM results reveal excess MWCNTs delay Bi_2WO_6 growing and reduced particle size, increasing the adsorption sites and avoiding nanotubes aggregation.

Moreover, the EDS technique was employed to estimate the chemical composition of resulted flower-like structure of pure Bi_2WO_6, as seen in **Fig. 3 a,b**. The outcomes reveal the weight percent of the product made up of only the Bi (47%), W (38%), and O (13%) elements signals occurred in the flower-like structure of Bi_2WO_6. **Fig. 3 b** shows further the weight percent of Bi_2WO_6/MWCNTs nanocomposite. The results from the EDS pattern analysis of Bi_2WO_6/MWCNTs proved the elements Bi, O, W, and C with weight percent about (28%,13%,20%, and 37), respectively, that confirmed embedded MWCNTs within the sample.

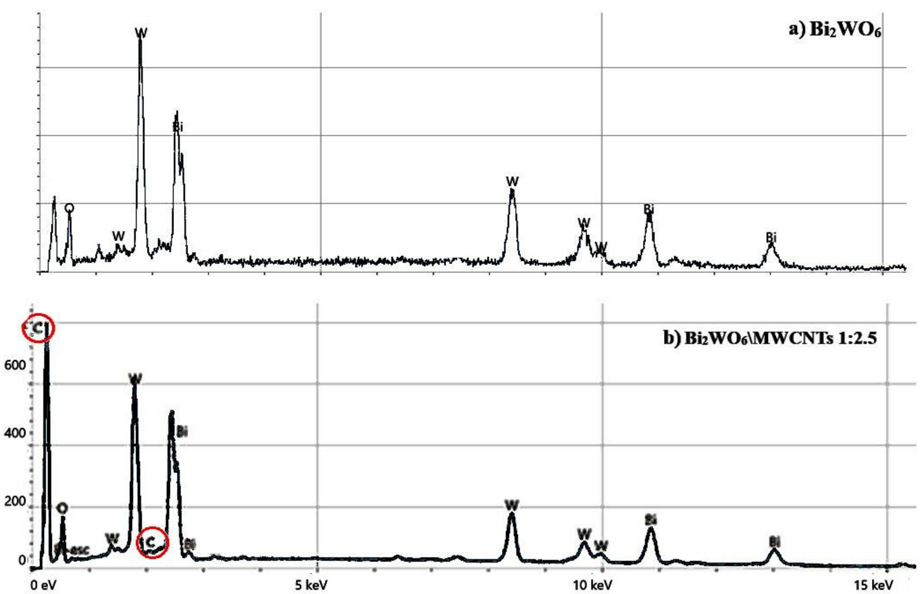

Figure 3: The EDS analysis of **a)** Bi_2WO_6 and **b)** Bi_2WO_6 /MWCNTs nanocomposite prepared by hydrothermal method.

As shown in **Fig. 4**, the antibacterial activity of pure Bi_2WO_6 and MWCNTs decorated Bi_2WO_6 at a molar ratio 1:2.5 of Bi_2WO_6: MWCNTs nanocomposite was evaluated at various concentrations (62.5, 125,250) µg/ml against Pseudomonas aeruginosa. Related to **Fig. 4**, the inhibition zones of Bi_2WO_6 /MWCNTs nanocomposite (A: control, E: 15.33, F: 17.2, G: 20.66) mm was higher than pure Bi_2WO_6 (A: control, B: 11.36, C: 13, D: 16.7) mm. Besides, it was found that the inhibitory effect of Bi_2WO_6 and nanocomposite increased as the concentration increased at 250 µg/ml, as shown in **Fig. 4**.

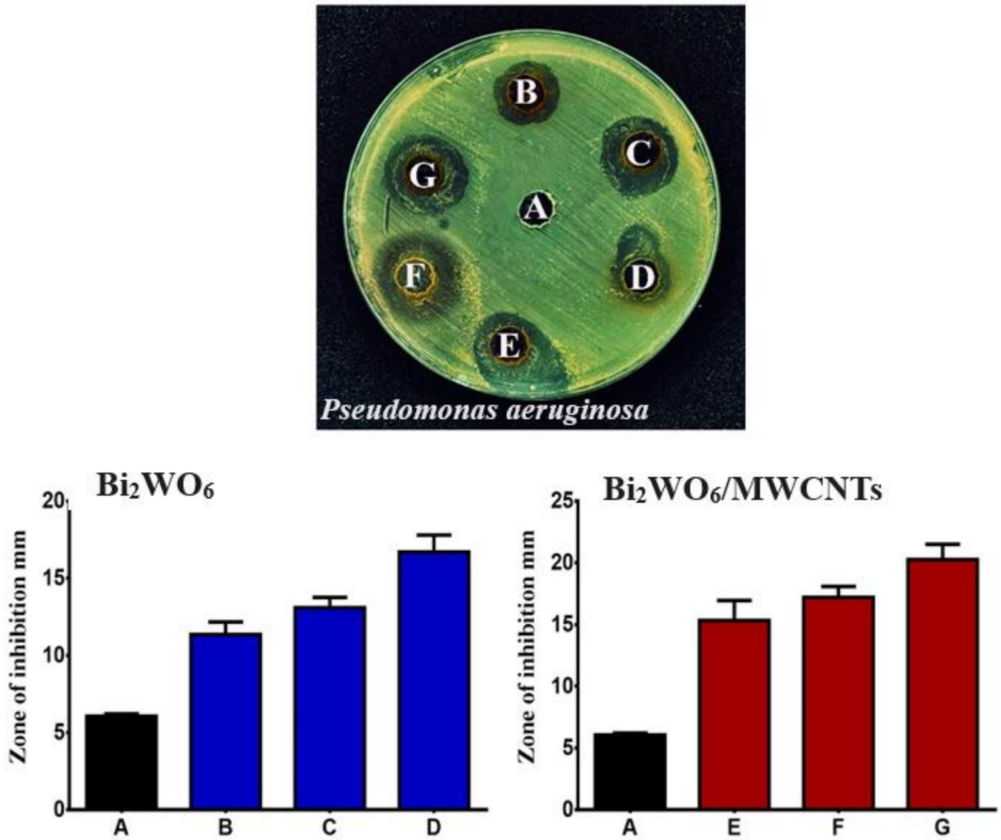

Figure 4: Image of inhibition zone (upper panel) of pure Bi_2WO_6 (A,B,C,D) and Bi_2WO_6 /MWCNTs (A,E,F,G) and antibacterial activity of pure Bi_2WO_6 (left pane) and Bi_2WO_6 /MWCNTs (right panel) at molar ratio 1:2.5 of Bi_2WO_6: MWCNTs against Pseudomonas aeruginosa using different content: **a**) control untreated bacterial strain. **b)** Bacteria treated with 62.5 µg/ml of Bi_2WO_6. **c**) Bacteria treated with 125 µg/ml of Bi_2WO_6. **d**) Bacteria treated with 250 µg/ml of Bi_2WO_6. **e**) Bacteria treated with 62.5 µg/ml of Bi_2WO_6/MWCNTs. **f**) Bacteria treated with 125 µg/ml of Bi_2WO_6/MWCNTs. **g**) Bacteria treated with 250 µg/ml of Bi_2WO_6/MWCNTs. Data are represented as mean ±SD of three independent experiments.

It is worth noting, that the higher antibacterial activity of Bi_2WO_6/MWCNTs nanocomposite is attributed to the high aspect ratio and surface area of MWCNTs. The results reveal that the embedded MWCNTs caused damage to the cell membrane of bacteria due to the fibrous structure of MWCNTs that provide higher accessible surface area and then release their DNA content [50-51].

The ability of pure Bi_2WO_6 and nanocomposite Bi_2WO_6/MWCNTs at molar ratio 1:2.5 of Bi_2WO_6: MWCNTs in the inhabited biofilm of formation Pseudomonas aeruginosa was displayed in **Fig. 5**, respectively. In this test, the nanocomposite showed more effectiveness in biofilm-reduced formation than pure Bi_2WO_6. Research indicates that reactive oxygen species (ROS) have a role in biofilm reduction by oxidizing cell membranes, which in turn changes fluid permeability and ion transport and inhibits metabolic formation [52].

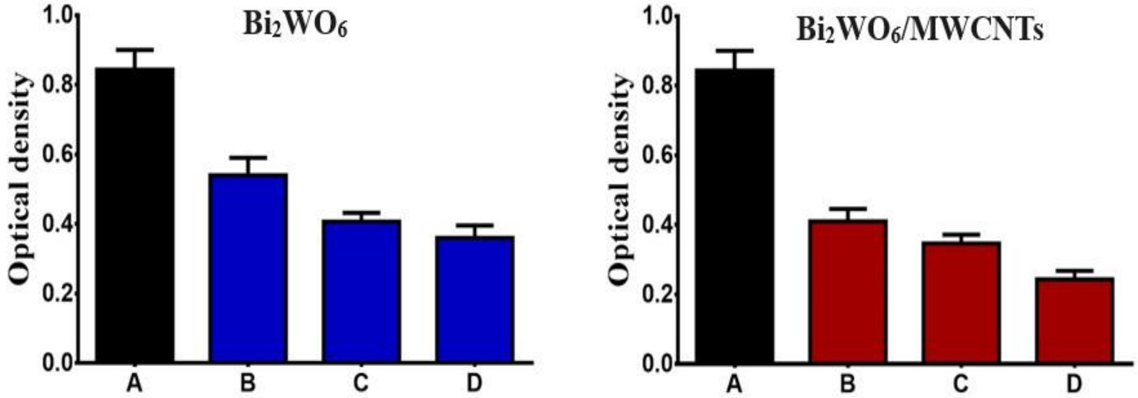

Figure 5: Bi_2WO_6 (left panel)and Bi_2WO_6/MWCNTs (right panel) at molar ratio 1:2.5 of Bi_2WO_6: MWCNTs reduce biofilm formation of Pseudomonas aeruginosa at different content: **a)** control untreated bacterial strains. **b)** Bacterial treated with 62.5 µg/ml. **c)** Bacteria treated with 125 µg/ml. **d)** Bacteria treated with 250 µg/ml of. Data are represented as mean ±SD

The confocal fluorescence imaging method (Olympus model, Japan) examined how bacterial biofilm inhibition was affected by pure Bi_2WO_6 and nanocomposite. In this test, the biofilm kit was used to provide wo color fluorescence stains to discriminate between the live and dead of Pseudomonas aeruginosa bacteria based on the membrane integrity, as shown in **Fig. 6 a,b,c**. Using green fluorescent protein (SYTO9) to stain healthy membranes and red fluorescent protein (propidium iodide) to stain bacterial strains responsible for membrane damage, it can be possible to discriminate between the live and dead cells. As shown in **Fig. 6 a**, the untreated biofilm bacterial strain (A: control) displays green fluorescence of complete bacteria. In the sate of treated biofilm with resulted samples, the bacterial strains display orange to red fluorescence, as shown in **Fig. 6 c,d** of pure Bi_2WO_6 and nanocomposite, respectively. In comparison to untreated bacterial strains with a biofilm structure, these results show that bacterial biofilms are damaged and that dead bacterial strains are present after treatment with pure Bi_2WO_6 and Bi_2WO_6/MWCNTs nanocomposite at a concentration of 125 µg/ml, which is associated with oxidative stress.

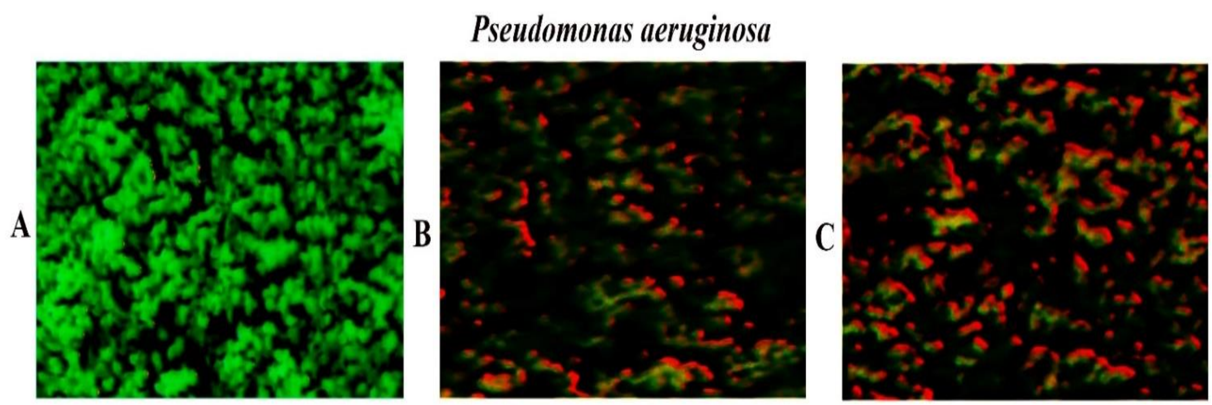

Figure 6: Reduction of bacterial biofilm formation of P. aeruginosa. **a)** Untreated control bacteria. **b)** Bacteria treated with pure Bi_2WO_6 and **c)** Bi_2WO_6/MWCNTs at molar ratio 1:2.5 of Bi_2WO_6: MWCNTs.

In addition, the values of the mass absorption coefficients that were obtained [17] are of great significance. These coefficients were determined based on the density of the material, which is 2.7g/cm3, and the thickness of the Aluminum, which is 5 cm. Subsequently, the linear absorption coefficient, which is a crucial parameter, was calculated and presented in **Table 1**. Furthermore, an equation was derived from this data in order to compute the linear absorption coefficients for any given energy. This equation allows for a comprehensive understanding of the relationship between the energy and the absorption coefficients, facilitating further analysis and exploration in this field.

4. Conclusions

The conclusion of this work represented synthesized pure Bi_2WO_6 and Bi_2WO_6/MWCNTs nanocomposite with the molar ratio of 1:2.5 of Bi_2WO_6: MWCNTs via facile hydrothermal method. The FTIR analysis confirmed the chemical bonding within the nanostructure, with additional peaks observed for the nanocomposite related to decoration and embedded MWCNTs. FESEM images revealed that introducing MWCNTs reduced nanoparticle aggregation, resulting in smaller particle sizes and increased adsorption sites compared to pure Bi_2WO_6. The EDS analysis confirmed embedded MWCNTs within the sample. Besides, the antibacterial activity test demonstrated that Bi_2WO_6/MWCNTs nanocomposite exhibited higher inhibition zones against gram-negative Pseudomonas ariginosa compared to pure Bi_2WO_6. The high aspect ratio makes MWCNTs disrupt the bacterial cell membrane and death cell. Additionally, the resulting samples effectively reduced bacteria biofilm formation, with nanocomposite showing higher anti-biofilm activity due to the ROS generation inducing oxidative stress.

Conflict of Interest

The authors declare that they have no conflict of interest.

References

[1] N. D. Phu, L. H. Hoang, X.-B. Chen, M.-H. Kong, H.-C. Wen, and W. C. Chou, "Study of photocatalytic activities of Bi_2WO_6 nanoparticles synthesized by fast microwave-assisted method," *Journal of Alloys and Compounds,* vol. 647, pp. 123-128, 2015.

[2] Y. Huang, Z. Ai, W. Ho, M. Chen, and S. Lee, "Ultrasonic spray pyrolysis synthesis of porous Bi2WO6 microspheres and their visible-light-induced photocatalytic removal of NO," *The Journal of Physical Chemistry C,* vol. 114, no. 14, pp. 6342-6349, 2010.

[3] F. Amano, K. Nogami, and B. Ohtani, "Visible light-responsive bismuth tungstate photocatalysts: effects of hierarchical architecture on photocatalytic activity," *The Journal of Physical Chemistry C,* vol. 113, no. 4, pp. 1536-1542, 2009.

[4] G. Zhao, S. Liu, Q. Lu, F. Xu, and H. Sun, "Fabrication of electrospun Bi_2WO_6 microbelts with enhanced visible photocatalytic degradation activity," *Journal of alloys and compounds,* vol. 578, pp. 12-16, 2013.

[5] D. Wu, H. Zhu, C. Zhang, and L. Chen, "Novel synthesis of bismuth tungstate hollow nanospheres in water–ethanol mixed solvent," *Chemical communications,* vol. 46, no. 38, pp. 7250-7252, 2010.

[6] X. Hong, Y. Li, X. Wang, J. Long, and B. Liang, "Carbon nanosheet/MnO_2/BiOCl ternary composite for degradation of organic pollutants," *Journal of Alloys and Compounds,* vol. 891, p. 162090, 2022.

[7] C. Chen *et al.*, "Adsorption, photocatalytic and sunlight-driven antibacterial activity of Bi_2WO_6/graphene oxide nanoflakes," *Vacuum,* vol. 116, pp. 48-53, 2015.

[8] M. Zhang *et al.*, "Ultrathin Bi_2WO_6 nanosheets loaded g-C_3N_4 quantum dots: A direct Z-scheme photocatalyst with enhanced photocatalytic activity towards degradation of organic pollutants under wide spectrum light irradiation," *Journal of colloid and interface science,* vol. 539, pp. 654-664, 2019.

[9] J. Ren, W. Wang, M. Shang, S. Sun, and E. Gao, "Heterostructured bismuth molybdate composite: preparation and improved photocatalytic activity under visible-light irradiation," *ACS applied materials & interfaces,* vol. 3, no. 7, pp. 2529-2533, 2011.

[10] Z. Zhang, W. Wang, L. Wang, and S. Sun, "Enhancement of visible-light photocatalysis by coupling with narrow-band-gap semiconductor: a case study on Bi_2S_3/Bi_2WO_6," *ACS applied materials & interfaces,* vol. 4, no. 2, pp. 593-597, 2012.

[11] M.-S. Gui, W.-D. Zhang, Y.-Q. Chang, and Y.-X. Yu, "One-step hydrothermal preparation strategy for nanostructured WO_3/Bi_2WO_6 heterojunction with high visible light photocatalytic activity," *Chemical Engineering Journal,* vol. 197, pp. 283-288, 2012.

[12] X. Li *et al.*, "A templated method to Bi_2WO_6 hollow microspheres and their conversion to double-shell Bi2O3/Bi2WO6 hollow microspheres with improved photocatalytic performance," *Inorganic Chemistry,* vol. 51, no. 11, pp. 6245-6250, 2012.

[13] Z.-Q. Li, X.-T. Chen, and Z.-L. Xue, "Microwave-assisted synthesis and photocatalytic properties of flower-like Bi_2WO_6 and Bi_2O_3–Bi_2WO_6 composite," *Journal of colloid and interface science,* vol. 394, pp. 69-77, 2013.

[14] Z. Wei and Y. Zhu, "Synthesis and performance enhancement for Bi_2WO_6 as high-activity visible-light-driven photocatalysts," *Nanostructured Photocatalysts: Advanced Functional Materials,* pp. 359-389, 2016.

[15] J. Tian, Z. Zhu, and B. Liu, "Novel Bi_2MoO_6/Bi_2WO_6/MWCNTs photocatalyst with enhanced photocatalytic activity towards degradation of RB-19 under visible light irradiation," *Colloids and Surfaces A: Physicochemical and Engineering Aspects,* vol. 581, p. 123798, 2019.

[16] Y. Liu, C. Nie, X. Liu, X. Xu, Z. Sun, and L. Pan, "Review on carbon-based composite materials for capacitive deionization," *Rsc Advances,* vol. 5, no. 20, pp. 15205-15225, 2015.

[17] Z. Lv, H. Zhou, H. Liu, B. Liu, M. Liang, and H. Guo, "Controlled assemble of oxygen vacant CeO_2@ Bi_2WO_6 hollow magnetic microcapsule heterostructures for visible-light photocatalytic activity," *Chemical Engineering Journal,* vol. 330, pp. 1297-1305, 2017.

[18] Y. Li, J. Liu, X. Huang, and J. Yu, "Carbon-modified Bi_2WO_6 nanostructures with improved photocatalytic activity under visible light," *Dalton Transactions,* vol. 39, no. 14, pp. 3420-3425, 2010.

[19] Q. Xiang, J. Yu, and M. Jaroniec, "Graphene-based semiconductor photocatalysts," *Chemical Society Reviews,* vol. 41, no. 2, pp. 782-796, 2012.

[20] D. S. Ahmed, M. K. Mohammed, and M. R. Mohammad, "Sol–gel synthesis of Ag-doped titania-coated carbon nanotubes and study their biomedical applications," *Chemical Papers,* vol. 74, no. 1, pp. 197-208, 2020.

[21] M. K. Mohammed, Z. J. Taqi, A. M. A. Hassen, M. S. Jabir, and D. S. Ahmed, "SWCNTs/ZnO-Ag/ZnO-Au nanocomposite increases bactericidal activity of phagocytic cells against Staphylococcus aureus," in *AIP Conference Proceedings*, 2021, vol. 2372, no. 1: AIP Publishing.

[22] H. N. Abid, A. Al-Keisy, D. S. Ahmed, and S. Singh, "Preparation and Characterization of Bi2MO6 (M= Mo, W) for Antibacterial Activity," *Journal of Applied Sciences and Nanotechnology,* vol. 3, no. 2, 2023.

[23] A. Elhissi, W. Ahmed, I. U. Hassan, V. Dhanak, and A. D'Emanuele, "Carbon nanotubes in cancer therapy and drug delivery," *Journal of drug delivery,* vol. 2012, 2012.

[24] K. A. Wepasnick, B. A. Smith, J. L. Bitter, and D. Howard Fairbrother, "Chemical and structural characterization of carbon nanotube surfaces," *Analytical and bioanalytical chemistry,* vol. 396, pp. 1003-1014, 2010.

[25] D. Ahmed and A. Abed, "Controlled surface modification of CNTs using mild acids through powerful sonication technique," *Acta Physica Polonica,* vol. 134, pp. 7-9, 2018.

[26] Z. Liu, X. Sun, N. Nakayama-Ratchford, and H. Dai, "Supramolecular chemistry on water-soluble carbon nanotubes for drug loading and delivery," *ACS nano,* vol. 1, no. 1, pp. 50-56, 2007.

[27] N. Q Ali, A. A Taha, and D. S Ahmed, "Mg-doped NiO nanoparticles decorated multi-walled carbon nanotube (MWCNT) nanocomposite and their biological activities," *Journal of Nanostructures,* vol. 11, no. 2, pp. 276-285, 2021.

[28] D. S Ahmed, A. L Abed, A. J Bohan, and J. Y Rbat, "Effect of (ZnO/MWCNTs) hybrid concentrations on microbial pathogens removal," *Engineering and Technology Journal,* vol. 33, no. 8B, pp. 1402-1411, 2015.

[29] N. Ali, A. Taha, and D. S. Ahmed, "Characterization of treated multi-walled carbon nanotubes and antibacterial properties," *Journal of Applied Sciences and Nanotechnology,* vol. 1, no. 2, pp. 1-9, 2021.

[30] A. M. Aljeboree, S. A. Hussein, M. A. Jawad, and A. F. Alkaim, "Hydrothermal synthesis of eco-friendly ZnO/CNT nanocomposite and efficient removal of Brilliant Green cationic dye," *Results in Chemistry,* p. 101364, 2024.

[31] Z. R. Rhoomi, D. S. Ahmed, M. S. Jabir, B. Balasubramanian, M. A. Al-Garadi, and A. A. Swelum, "Facile Hydrothermal Synthesis of $BiVO_4$/MWCNTs Nanocomposites and Their Influences on the Biofilm Formation of Multidrug Resistance Streptococcus mutans and Proteus mirabilis," *ACS omega,* vol. 8, no. 40, pp. 37147-37161, 2023.

[32] E. Heydari-Bafrooei and S. Askari, "Electrocatalytic activity of MWCNT supported Pd nanoparticles and MoS_2 nanoflowers for hydrogen evolution from acidic media," *International Journal of Hydrogen Energy,* vol. 42, no. 5, pp. 2961-2969, 2017.

[33] S. Ye *et al.*, "MWCNT/$BiVO_4$ photocatalyst for inactivation performance and mechanism of Shigella flexneri HL, antibiotic-resistant pathogen," *Chemical Engineering Journal,* vol. 424, p. 130415, 2021.

[34] J. Wu, F. Duan, Y. Zheng, and Y. Xie, "Synthesis of Bi_2WO_6 nanoplate-built hierarchical nest-like structures with visible-light-induced photocatalytic activity," *The Journal of Physical Chemistry C,* vol. 111, no. 34, pp. 12866-12871, 2007.

[35] N. Hao *et al.*, "A sensitive photoelectrochemical (PEC) platform fabricated with nitrogen-doped graphene quantum dots decorated Bi_2WO_6 for detection of pentachlorophenol," *Journal of Electroanalytical*

Chemistry, vol. 801, pp. 410-415, 2017.
[36] G. Zhao, S. Liu, Q. Lu, and L. Song, "Controllable synthesis of Bi_2WO_6 nanofibrous mat by electrospinning and enhanced visible photocatalytic degradation performances," *Industrial & engineering chemistry research,* vol. 51, no. 31, pp. 10307-10312, 2012.
[37] Z. S. Seddigi *et al.*, "Facile synthesis of light harvesting semiconductor bismuth oxychloride nano photo-catalysts for efficient removal of hazardous organic pollutants," *PloS one,* vol. 12, no. 2, p. e0172218, 2017.
[38] G. Su, C. Yang, and J.-J. Zhu, "Fabrication of gold nanorods with tunable longitudinal surface plasmon resonance peaks by reductive dopamine," *Langmuir,* vol. 31, no. 2, pp. 817-823, 2015.
[39] F. Chen, D. Li, B. Luo, M. Chen, and W. Shi, "Two-dimensional heterojunction photocatalysts constructed by graphite-like C_3N_4 and Bi_2WO_6 nanosheets: enhanced photocatalytic activities for water purification," *Journal of Alloys and Compounds,* vol. 694, pp. 193-200, 2017.
[40] J. Yu, J. Xiong, B. Cheng, Y. Yu, and J. Wang, "Hydrothermal preparation and visible-light photocatalytic activity of Bi_2WO_6 powders," *Journal of Solid State Chemistry,* vol. 178, no. 6, pp. 1968-1972, 2005.
[41] H. Li, N. Li, M. Wang, B. Zhao, and F. Long, "Synthesis of novel and stable g-C_3N_4-Bi_2WO_6 hybrid nanocomposites and their enhanced photocatalytic activity under visible light irradiation," *Royal Society Open Science,* vol. 5, no. 3, p. 171419, 2018.
[42] X. Zhao, R. Liu, Z. Chi, Y. Teng, and P. Qin, "New insights into the behavior of bovine serum albumin adsorbed onto carbon nanotubes: comprehensive spectroscopic studies," *The journal of physical chemistry B,* vol. 114, no. 16, pp. 5625-5631, 2010.
[43] K. S. Khashan, G. M. Sulaiman, and R. Mahdi, "The effect of laser energy on the properties of carbon nanotube—iron oxide nanoparticles composite prepared via pulsed laser ablation in liquid," *Materials Research Express,* vol. 5, no. 10, p. 105004, 2018.
[44] Y. Zhou *et al.*, "Monolayered Bi_2WO_6 nanosheets mimicking heterojunction interface with open surfaces for photocatalysis," *Nature communications,* vol. 6, no. 1, p. 8340, 2015.
[45] C. C. Mardare, D. Tanasic, A. Rathner, N. Müller, and A. W. Hassel, "Growth inhibition of Escherichia coli by zinc molybdate with different crystalline structures," *physica status solidi (a),* vol. 213, no. 6, pp. 1471-1478, 2016.
[46] K. S. Khashan, F. A. Abdulameer, M. S. Jabir, A. A. Hadi, and G. M. Sulaiman, "Anticancer activity and toxicity of carbon nanoparticles produced by pulsed laser ablation of graphite in water," *Advances in Natural Sciences: Nanoscience and Nanotechnology,* vol. 11, no. 3, p. 035010, 2020.
[47] D. T. Danielson, D. K. Sparacin, J. Michel, and L. C. Kimerling, "Surface-energy-driven dewetting theory of silicon-on-insulator agglomeration," *Journal of applied physics,* vol. 100, no. 8, 2006.
[48] G. Bluvol, M. Kässberger, and F. Reichhart, "Optimizing Solids and Rheology in Blade Coating Using Pigment Blends—Part 1," *O PAPEL,* vol. 11, pp. 55-59, 2011.
[49] L. Fiiipponi and D. Sutherland, *Nanotechnologies: principles, applications, implications and hands-on activities: A compendium for educators*. European Union, Directorate General for Research and Innovation, 2012.
[50] E. M. Elsehly, N. Chechenin, A. Makunin, H. Motaweh, and E. Leksina, "Functionalized carbon nanotubes based filters for chromium removal from aqueous solutions," *Water Science and Technology,* vol. 75, no. 7, pp. 1564-1571, 2017.
[51] M. K. d. N. S. Leandro *et al.*, "Characterization and evaluation of layered Bi_2WO_6 nanosheets as a new antibacterial agent," *Antibiotics,* vol. 10, no. 9, p. 1068, 2021.
[52] J. Zhao *et al.*, "Electrospinning construction of Bi_2WO_6/RGO composite nanofibers with significantly enhanced photocatalytic water splitting activity," *RSC advances,* vol. 6, no. 69, pp. 64741-64748, 2016.